

Removing the Microlensing Blending-Parallax Degeneracy Using Source Variability

R.J. Assef¹, A. Gould¹,
and

C. Afonso^{2,5}, J.N. Albert³, J. Andersen⁴, R. Ansari³, É. Aubourg⁵, P. Bareyre⁵,
J.P. Beaulieu⁶, X. Charlot⁵, C. Coutures^{5,6}, R. Ferlet⁶, P. Fouqué^{7,8}, J.F. Glicenstein⁵,
B. Goldman^{2,5}, D. Graff^{9,1}, M. Gros⁵, J. Haissinski³, C. Hamadache⁵, J. de Kat⁵, L. Le
Guillou^{10,5}, É. Lesquoy^{5,6}, C. Loup⁶, C. Magneville⁵, J.B. Marquette⁶, É. Maurice¹¹,
A. Maury^{12,8}, A. Milsztajn⁵, M. Moniez³, N. Palanque-Delabrouille⁵, O. Perdureau³, Y.R.
Rahal³, J. Rich⁵, M. Spiro⁵, P. Tisserand⁵, A. Vidal-Madjar⁶, L. Vigroux^{5,6}, S. Zylberajch⁵

(The EROS-2 Collaboration)

D.P. Bennett^{13,17,18}, A. C. Becker¹⁴, K. Griest¹⁵, T. Vandehei¹⁵, D.L. Welch¹⁶

(For the MACHO Collaboration)

A. Udalski¹⁹, M.K. Szymański¹⁹, M. Kubiak¹⁹, G. Pietrzyński^{19,20}, I. Soszyński^{19,20},
O. Szewczyk¹⁹, Ł. Wyrzykowski^{19,21}

(The OGLE Collaboration)

¹Department of Astronomy, Ohio State University, 140 W. 18th Ave., Columbus, OH 43210, USA;
rjassemf,gould@astronomy.ohio-state.edu

²Max-Planck-Institut für Astronomie, Koenigstuhl 17,D-69117 Heidelberg, Germany;
afonso@mpia-hd.mpg.de,goldman@mpia-hd.mpg.de

³Laboratoire de l’Accélérateur Linéaire, IN2P3 CNRS, Université de Paris-Sud, 91405 Orsay Cedex, France;
albert,ansari,jhaiss,moniez,perderos,rahal@lal.in2p3.fr,marquett@iap.fr

⁴The Niels Bohr Institute, Copenhagen University, Juliane Maries Vej 30, DK2100 Copenhagen, Denmark;
JA@ASTRO.KU.DK

⁵CEA, DSM, DAPNIA, Centre d’Études de Saclay, 91191 Gif-sur-Yvette Cedex, France;
charlot,coutures,glicens,Michel.Gros,cmv,mimile,nathalie,rich,tisseran@hep.saclay.cea.fr;
eric@aubourg.net,pierre.bareyre@cdf.in2p3.fr,clarisse.hamadache@cdf.in2p3.fr,jean.dekat@antigone.cea.fr,
lesquoy@in2p3.fr,alain@spaceobs.com,mspiro@admin.in2p3.fr,zylberajch@wanadoo.fr

⁶Institut d’Astrophysique de Paris, INSU CNRS, 98 bis Boulevard Arago, 75014 Paris, France;
beaulieu,ferlet,loup,alfred,vigroux@iap.fr

⁷Observatoire Midi-Pyrénées, Laboratoire d’Astrophysique (UMR 5572), 14 av. E. Belin, 31400 Toulouse, France; pfouque@ast.obs-mip.fr

⁸European Southern Observatory (ESO), Casilla 19001, Santiago 19, Chile

⁹Division of Medical Imaging Physics, Johns Hopkins University Baltimore, MD 21287-0859, USA;
dgraff3@jhmi.edu

¹⁰Instituut voor Sterrenkunde, Celestijnenlaan 200 B, B-3001 Leuven,Belgium;
Laurent.LeGuillou@ster.kuleuven.be

¹¹Observatoire de Marseille, 2 place Le Verrier, 13248 Marseille Cedex 04, France;
eric.maurice@oamp.fr

¹²San Pedro de Atacama Celestial Exploration, Casilla 21, San Pedro de Atacama, Chile

¹³ Microlensing Observations for Astrophysics (MOA) Collaboration

¹⁴Department of Astronomy, University of Washington, Box 351580, Seattle, WA 98195;
becker@astro.washington.edu

¹⁵Physics Dept. 0319, University of California, San Diego, La Jolla CA 92093;
kgriest@ucsd.edu, vandehei@sbcglobal.net

¹⁶Department of Physics & Astronomy, McMaster University, Hamilton, Ontario Canada L8S 4M1;
welch@physics.mcmaster.ca

¹⁷Probing Lensing Anomalies NETwork (PLANET) Collaboration

¹⁸Department of Physics, Notre Dame University, Notre Dame, IN 46556, USA;
bennett@nd.edu

¹⁹Warsaw University Observatory, Al. Ujazdowskie 4, 00-478 Warszawa, Poland;

ABSTRACT

Microensing event MACHO 97-SMC-1 is one of the rare microensing events for which the source is a variable star, simply because most variable stars are systematically eliminated from microensing studies. Using observational data for this event, we show that the intrinsic variability of a microlensed star is a powerful tool to constrain the nature of the lens by breaking the degeneracy between the microlens parallax and the blended light. We also present a statistical test for discriminating the location of the lens based on the χ^2 contours of the vector $\mathbf{\Lambda}$, the inverse of the projected velocity. We find that while SMC self lensing is somewhat favored over halo lensing, neither location can be ruled out with good confidence.

Subject headings: gravitational lensing — stars: variables: other

1. Introduction

Microensing parallax measurements are a potentially powerful way to constrain the nature of the lenses. For typical events, the only measured parameter that is related to the underlying physical properties of the lens is the Einstein timescale t_E . However, this relation is rather indirect,

$$t_E = \frac{\theta_E}{\mu_{\text{rel}}}, \quad \theta_E = \sqrt{\kappa M \pi_{\text{rel}}} \quad (1)$$

where π_{rel} and μ_{rel} are the lens-source relative parallax and proper motion, θ_E is the angular Einstein radius, M is the mass of the lens, and $\kappa \equiv 4G/c^2 \text{AU} \sim 8.14 \text{ mas } M_{\odot}^{-1}$. That is, t_E is effectively a combination of three parameters describing the lens and the source: M , π_{rel} , and μ_{rel} . If one can also measure the Einstein radius projected onto the observer plane, \tilde{r}_E , or equivalently the microlens parallax,

$$\pi_E = \frac{\text{AU}}{\tilde{r}_E} = \sqrt{\frac{\pi_{\text{rel}}}{\kappa M}}, \quad (2)$$

udalski@astrouw.edu.pl

²⁰Universidad de Concepción, Departamento de Física, Casilla 160–C, Concepción, Chile

²¹Institute of Astronomy Cambridge University, Madingley Rd., CB3 0HA Cambridge, UK;
wyrzykow@ast.cam.ac.uk

then this three-fold degeneracy can be reduced by one dimension, allowing better constraints on the mass. Moreover, one can disentangle the mass from the kinematic variables and so extract a purely kinematic quantity, the projected velocity,

$$\tilde{v} = \frac{\tilde{r}_E}{t_E} = \frac{\text{AU}\mu_{\text{rel}}}{\pi_{\text{rel}}}. \quad (3)$$

This quantity is particularly useful for understanding the nature of the lenses detected toward the Magellanic Clouds (MCs), which is currently under debate. The MACHO collaboration (Alcock et al. 2000) detected 13 to 17 such events and argued that the majority of these were due to MACHOs making up about 20% of the Milky Way dark halo, whereas the EROS collaboration (Afonso et al. 2003; Tisserand & Milsztajn 2005) argued that their relative lack of such detections was consistent with all the events being due to stars in the Milky Way disk or the MCs themselves. All events detected so far toward the SMC have been very bright, even though the detection of fainter events was expected. We recognize this statistical issue but we will not address it any further on this work. One way to determine the nature of individual lenses is to measure their parallax π_E and so their projected velocity \tilde{v} . Bouteux & Gould (1996) showed that this quantity differs greatly depending on the lens population: $\sim 50 \text{ km s}^{-1}$ for lenses in the Galactic disk, $\sim 300 \text{ km s}^{-1}$ for halo lenses, and $\sim 2000 \text{ km s}^{-1}$ for lenses within the MCs themselves.

However, to date it has been possible to measure microlens parallaxes for only a handful of events (Poindexter et al. 2005 and references therein). Measurement requires that one compare \tilde{r}_E to some “standard ruler” in the observer plane, which must therefore be of comparable size to this quantity, i.e., of order 1 AU. While π_E could be routinely measured by comparing the microlensing event as observed from the Earth and from a satellite in solar orbit (Refsdal 1966), the only standard ruler generally available for ground-based observations is the Earth’s orbit itself. Hence, unless the event takes a substantial fraction of a year (in practice $t_E \gtrsim 90$ days), it is rarely possible to measure its parallax.

The problem is that the microlens parallax is actually a 2-dimensional vector quantity, $\boldsymbol{\pi}_E$, whose magnitude is π_E and whose direction is that of the lens motion relative to the source. The component of $\boldsymbol{\pi}_E$ parallel to the direction of the Sun at the peak of the event, $\pi_{E,\parallel}$, induces a distortion in the light curve that is asymmetric with respect to the peak, while the other component, $\pi_{E,\perp}$, induces a symmetric distortion. While $\pi_{E,\parallel}$ is relatively easy to measure, even for comparatively short events (Gould et al. 1994), $\pi_{E,\perp}$ is subject to various degeneracies, both discrete and continuous (Smith et al. 2003; An et al. 2004; Gould 2004).

The fundamental problem is that changes in any one of four of the five parameters that describe standard microlensing also induce symmetric distortions in the light curve, and the

combination of these can often mimic the effects of $\pi_{E,\perp}$. The light curve of a standard (non-parallax) microlensing event is modeled by

$$f_k(t) = f_{s,k}A[u(t)] + f_{b,k}, \quad (4)$$

where the magnification A is given by (Einstein 1936; Paczyński 1986),

$$A(u) = \frac{u^2 + 2}{u\sqrt{u^2 + 2}}, \quad (5)$$

and u is the source-lens separation in units of θ_E , which is given by the Pythagorean theorem,

$$u = \sqrt{\beta^2 + \tau^2} \quad (6)$$

in terms of τ and the impact parameter β ,

$$\tau(t) = \frac{t - t_0}{t_E}, \quad \beta = u_0. \quad (7)$$

Here $f_k(t)$ is the observed flux, $f_{s,k}$ is the flux of the microlensed source, and $f_{b,k}$ is the flux from any unlensed background light, all as observed at the k th observatory. Inspection of these equations shows that changes in u_0 , t_E , f_s and f_b all induce effects on the light curve that are symmetric with respect to t_0 .

If it were somehow possible to measure f_b independent of the light curve, then the problems posed by these degeneracies would be greatly reduced. First, since the baseline flux, $f_{\text{base}} = f_s + f_b$, is generally determined very precisely, measurement of f_b immediately yields f_s . Next, since the peak flux f_{peak} is also usually well measured, one can then also directly determine u_0 from $A(u_0) = (f_{\text{peak}} - f_b)/f_s$. This implies that only t_E and $\pi_{E,\perp}$ must really be simultaneously determined. Since changing these induces rather different light-curve distortions, it is relatively easy to disentangle them.

To date, three methods have been proposed to determine f_b : astrometry (Alard et al. 1995; Ghosh et al. 2004), precise imaging (Han 1997), and manipulation of a series of images using image subtraction (Gould & An 2002). These methods can all help, but they are fundamentally unable to resolve blended light due to a binary companion of the source that does not participate in the microlensing event. Such companions could lie at separations of order 10 AU, which corresponds to angular separations of order 1 mas or smaller. For the faint sources typical of microlensing events, this is too close to be resolved using current or foreseen instruments.

Here we propose a new method to resolve blended light. The method requires that the source be a regular variable, which is fairly rare for sources in typical microlensing fields.

However, the method does not suffer from the limitations of the other techniques: its ability to disentangle the source from the blended light works equally well regardless of their angular separation. We apply this technique to MACHO-97-SMC-1, which was a relatively long event whose source exhibited regular variability with an amplitude of about 3%. We show that this variability significantly constrains the blending and so improves the precision of the parallax measurement.

2. Data

MACHO 97-SMC-1 was discovered by the MACHO collaboration (Alcock et al. 1997) and independently by the EROS collaboration (Palanque-Delabrouille et al. 1998). The OGLE collaboration also observed the event during its late decline in its OGLE-II phase (Udalski et al. 1997a) and at baseline in its OGLE-III phase (Udalski 2003).

MACHO observations were mostly made at the dedicated 50" Great Melbourne telescope at Mount Stromlo, Australia from June 1993 to January 2000 with simultaneous imaging in “ V_M ” (4500–5900 Å) and “ R_M ” (5900–7800 Å) passbands, but also at CTIO in the Johnson-Cousins R filter from May through November 1997.

EROS observations were made at the dedicated 1m MARLY telescope at the European Southern Observatory at La Silla, Chile from July 1996 to February 2003 with simultaneous imaging in “ V_E ” (4200–7200 Å, peak at 5600 Å) and “ I_E ” (6200–9200 Å, peak at 7600 Å) wide passbands.

OGLE observations were made at the 1.3 meter Warsaw telescope at Las Campanas Observatory, Chile in Cousins I band from June 1997 to November 2000 for the OGLE-II phase and from June 2001 to August 2005 for the OGLE-III phase.

Because the OGLE-III observations began after the event was over, they cannot be used to directly constrain the microlensing event. We incorporate them only to better understand the variability. To this end, we fix the blending at a value similar to that of OGLE-II, since otherwise this parameter would be completely degenerate.

Afonso et al. (1999) showed that the source star is an intrinsic variable with a period of 5.126 days. They fit the event simultaneously for microlensing and intrinsic variations and used OGLE-II data to demonstrate that some of the apparent source in the EROS images was unrelated blended light and to better define the period of variability. The amplitude of these oscillations is so small (around 3% of the total flux) that the event was detected by EROS because it managed to survive their variable-star cuts. The MACHO collaboration

did not initially detect this event, mainly because their "main sequence variable" cut was still based on the LMC color-magnitude diagram and had not been corrected for the SMC. It was rather detected by coincidence while extracting variable stars for further study.

3. Parametrization

When a variable star is microlensed, the amplitude of the oscillations will be magnified by the same factor as the star's flux, completely independent of the amount of blended light. For example, if the star's variability period is much shorter than the event timescale, the ratio of the amplitude at baseline and at some magnified moment will yield a measurement of the magnification at that stage. Since this measurement is independent of the source's flux and of the blended light, knowing the magnification at some point allows one to solve the 2×2 system of equations formed by equation (4) at these two moments, thus disentangling the source from the blended light and so eliminating the degeneracy between the parallax and the blending.

In practice, measurements of the microlensing parameters are done by fitting a microlensing model to the observations, eliminating the requirement for the variability period to be much shorter than the event timescale. In this process, the magnified variability amplitude of the source will yield an extra constraint on the amount of blending to fit for the magnification at each stage, thereby breaking the forementioned degeneracy.

In this paper we fit the event to a standard microlensing model (eqs. [4]-[7]) plus parallax and combined with a variability model for the intrinsic variations of the source star. Following the procedure outlined by An et al. (2002), we model the effects of parallax by modifying equation (7),

$$\beta(t) = u_0 + \delta\beta, \quad \tau(t) = \frac{t - t_0}{t_E} + \delta\tau, \quad (8)$$

where

$$[\delta\tau(t), \delta\beta(t)] = [\boldsymbol{\pi}_E \cdot \Delta\mathbf{s}(t), \boldsymbol{\pi}_E \times \Delta\mathbf{s}(t)]. \quad (9)$$

and the parallax is evaluated in the geocentric frame. Here, $\Delta\mathbf{s}$ is the offset position of the Sun projected on the plane of the sky in the geocentric frame. The two components of $\boldsymbol{\pi}_E$ are free parameters of the model that we fit to the data. As in equation (7), t_0 is the time of the maximum, u_0 is the closest angular distance between the source and the lens in units of the angular Einstein radius, θ_E , and t_E is the Einstein timescale of the event.

Parallax models are generically subject to a four-fold discrete degeneracy (An et al. 2004; Gould 2004; Poindexter et al. 2005). Two solutions are related by the "constant

acceleration” degeneracy (Smith et al. 2003), which in the geocentric frame sends $u_0 \rightarrow -u_0$ and changes other parameters relatively little. The two other solutions are related by the “jerk-parallax” degeneracy, in which the jerk of the Earth’s motion can masquerade as a parallax effect (Gould 2004). Palanque-Delabrouille et al. (1998) found both constant-acceleration solutions, although they did not express them in exactly the terms presented here.

To describe the intrinsic variation of the star, we will begin by following Palanque-Delabrouille et al. (1998), who modeled the variability as a sine function, leaving as free parameters its angular frequency Ω , its phase ϕ , and its amplitude ϵ_k as measured at each observatory. Hence, the light curve is given by

$$f_k(t) = f_{s,k} A(t) [1 + \epsilon_k G(\Omega t + \phi)] + f_{b,k}, \quad G(x) \equiv \sin x. \quad (10)$$

Our approach is very similar, but with one minor modification. After we initially fit the light curve to equation (10), we fit the residuals to a fourth-order Fourier expansion to derive a new $G(x)$, which differs modestly from a sine function (see Fig. 1).

Udalski et al. (1997b) suggested that the light curve oscillations may be due to ellipsoidal variability of the source. If so, this would imply that the light curve should be subject to “xallarap” (binary-source motion) as well as parallax (Earth-motion) distortions. We will examine this possibility more closely in Appendix A, but for the present we simply treat these oscillations as an empirical fact of unknown origin.

4. Results

Using the model described in § 3, we fit simultaneously the data from all the observatory/filter combinations (7 in total). The χ^2 of the best fit, in total and by observatory/filter, is shown in Table 1 for the positive and negative u_0 solutions. It should be noted that the errors are scaled (with scaling factors 1.92, 2.65, 1, 0.79, 1.1, 0.75 and 1 respectively for each observatory as listed in Table 1) so that the best fit χ^2 is approximately equal to the number of data points in each observatory/filter. Also, the best fit parameters are listed in Table 2 with their respective errors for both solutions. We searched for the jerk-parallax solutions according to the prescription of Park et al. (2004). We indeed found two additional minima on the χ^2 surface, but these are excluded at the 12- σ and 28- σ levels respectively, and so they will not be further considered.

Parallax parameters are of special interest to constrain the lens projected velocity and mass. Their best fit values show that there is very little, if any, parallax effect. In Figure 2, we show χ^2 contours for both ($\pm u_0$) solutions. Although the χ^2 of the best fits do not

differ significantly, the errors are a factor 2-3 smaller for positive u_0 . In each case, the best fit variability period for the star is 5.1252 ± 0.0001 days, compatible with, but much more precise than, the ones found by Palanque-Delabrouille et al. (1998) and Udalski et al. (1997b).

Palanque-Delabrouille et al. (1998) raised the question of whether it is the microlensed source that is varying or it is the blended light. Their data alone permitted them to discriminate against the second option just at the $2.5\text{-}\sigma$ level. By including the data from all 7 observatories we find that the variable blended-light model is ruled out at the $7\text{-}\sigma$ level, so it will not be further considered.

In order to evaluate the role of the intrinsic source variations in constraining the blended flux, and so $\pi_{E,\perp}$, we remove the best-fit variation from the data and then refit these adjusted data using a standard microlensing model with parallax but with no oscillations. The χ^2 and the best fit parameters are summarized in Tables 1 and 2 respectively, for the $\pm u_0$ solutions. Note that the best fit for the parameters that are correlated with $\pi_{E,\perp}$, namely u_0 , t_E , $f_{s,k}$ and $f_{b,k}$, have changed somewhat compared with the variability-model best fit, but the main effect is that their errors have increased by a factor of 2-3 while the χ^2 of the best fit is virtually the same. This is reflected in the difference between the left and right contour plots of Figure 2, which respectively do and do not take variability into account. The contours on the right are strongly stretched in the direction of $\pi_{E,\perp}$ (note that $\pi_{E,\parallel}$ points just $2^\circ.2$ north of west, so $\pi_{E,\perp}$ is virtually the same as $\pi_{E,N}$). This demonstrates that if the source star is a regular variable, the degeneracy between $\pi_{E,\perp}$ and f_b can be broken and their values can be better constrained.

Wyrzykowski et al. (2006) searched the entire OGLE-III database up through the 2004 season for microlensing events with variable baselines. Out of about 1400 events, there were 21 with periodic variable baselines and 111 that showed a baseline with irregular variability. The latter are not well suited for this method, in part because apparent "microlensing events" on irregular variables can in principle be just a manifestation of their variability and in part because the amplitude of variability during the event cannot be precisely determined from the baseline variability. Naively, one would expect that half of the periodic ones were due to a variable source and half due to variable blend, which translates into an expectation of a little less than 1 regular variable source microlensing event for every 100 events detected. When considering also the probability of detecting parallax asymmetries on the light curve, the number of events to which the method presented in this paper is applicable is somewhat smaller. So, even though events like MACHO 97-SMC-1 are rare, there should be a fair number of cases for which the analysis described in this paper would prove useful.

5. Lens Location

A better constraint on the parallax parameters also gives a better constraint on the lens location, since the projected velocity of the lens depends directly on them (eqs. [2] and [3]). Figure 3 shows the χ^2 contours of the vector $\mathbf{\Lambda}$,

$$\mathbf{\Lambda} \equiv \frac{\tilde{\mathbf{v}}}{\tilde{v}^2} = \frac{\boldsymbol{\pi}_E t_E}{\text{AU}}, \quad (11)$$

whose direction is the same as the projected velocity but with the inverse of its magnitude. We choose this vector instead of the projected velocity because it is well behaved at high velocities and makes the contours clearer. Indeed if the best fit for t_E were independent of $\boldsymbol{\pi}_E$, the $\mathbf{\Lambda}$ contours would differ from the $\boldsymbol{\pi}_E$ contours just by a scale factor. Note, however, that these χ^2 contours are made in the frame of the Sun, rather than in the geocentric frame in which we conducted the parallax analysis. That is, we convert

$$\tilde{\mathbf{v}}_{hel} = \tilde{\mathbf{v}}_{geo} + \mathbf{v}_{\oplus, \perp}, \quad (12)$$

where $\mathbf{v}_{\oplus, \perp} = (29.75, 3.10) \text{ km s}^{-1}$ is the offset between the two frames. The inner circle shows $\tilde{v} = 2000 \text{ km s}^{-1}$ while the outer one shows $\tilde{v} = 300 \text{ km s}^{-1}$.

There are three possible locations for a lens that magnifies a star in the SMC: it is located either in the Milky Way disk, the Milky Way halo (halo lensing) or in the SMC itself (SMC self lensing). However, a disk location is immediately ruled out by the high projected velocity. At first sight, since the minimum χ^2 is located around a projected velocity of 1000 km s^{-1} for both u_0 solutions, SMC self lensing appears more probable, because this would seem to be a too high velocity for a halo lens. To quantitatively discriminate between these two possibilities, we compare the mean maximum likelihood parameter, $\langle \exp[-\Delta\chi^2/2] \rangle$, for halo and SMC lenses based on the χ^2 contours of their $\mathbf{\Lambda}$ vectors and their respective velocity distributions. We consider SMC self lensing and halo lensing in turn.

5.1. SMC Self Lensing

We begin by assuming that SMC lenses are Gaussian-distributed, namely, that they have a projected velocity probability distribution given by

$$P(\tilde{v}) d\tilde{v}_x d\tilde{v}_y \propto e^{-(\tilde{v}/\sigma)^2/2} \tilde{v} d\tilde{v}_{\text{North}} d\tilde{v}_{\text{East}}, \quad (13)$$

where σ is the velocity dispersion of the lenses. Then, the mean likelihood parameter is

$$\langle e^{-\Delta\chi^2/2} \rangle = \int e^{-\Delta\chi^2(\tilde{\mathbf{v}})/2} e^{-(\tilde{v}/\sigma)^2/2} \tilde{v} d\tilde{v}_{\text{North}} d\tilde{v}_{\text{East}} / \int e^{-(\tilde{v}/\sigma)^2/2} \tilde{v} d\tilde{v}_{\text{North}} d\tilde{v}_{\text{East}}. \quad (14)$$

The typical projected velocity of a SMC lens is not very clear but should be of the order of $\tilde{v} \gtrsim 1000 \text{ km s}^{-1}$, so we consider two different estimates for the velocity dispersion: $\sigma = 1000/\sqrt{2} \text{ km s}^{-1}$ and $\sigma = 3000/\sqrt{2} \text{ km s}^{-1}$. As mentioned above, the χ^2 calculation is more stable in $\mathbf{\Lambda}$ space, so we evaluate equation (14) in this space:

$$\langle e^{-\Delta\chi^2/2} \rangle = \int e^{-\Delta\chi^2(\mathbf{\Lambda})/2} e^{-(\tilde{v}/\sigma)^2/2} \Lambda^{-5} d\Lambda_{\text{North}} d\Lambda_{\text{East}} / \int e^{-(\tilde{v}/\sigma)^2/2} \Lambda^{-5} d\Lambda_{\text{North}} d\Lambda_{\text{East}}, \quad (15)$$

where $\Delta\chi^2(\mathbf{\Lambda})$ is taken directly from the data of the contour plots of Figure 3.

5.2. Halo Lensing

The calculation of the mean likelihood parameter for halo lensing is very similar to the one performed for SMC self lensing in the previous section, but we must allow for two considerations that were implicitly neglected before: the spatial distribution of the lenses and the effect of the Sun's and the source's motions on the projected velocity of the lens. We assume that halo lenses are distributed in an isothermal sphere,

$$\rho(r) = \frac{1}{a_0^2 + r^2}, \quad (16)$$

where r is the lens Galactocentric distance and where we adopt $a_0 = 5 \text{ kpc}$ for the core radius and assume that the Sun is at $R_0 = 7.6 \text{ kpc}$. The velocity probability distribution is then weighted by the density of lenses at each distance and by the size of its respective Einstein ring, and integrated over all possible distances, giving a mean likelihood parameter of

$$\langle e^{-\Delta\chi^2/2} \rangle = \int \exp[-\Delta\chi^2(\mathbf{\Lambda})/2] g(\mathbf{\Lambda}, D_L) dD_L d\Lambda_{\text{North}} d\Lambda_{\text{East}} / \int g(\mathbf{\Lambda}, D_L) dD_L d\Lambda_{\text{North}} d\Lambda_{\text{East}}, \quad (17)$$

where

$$g(\mathbf{\Lambda}, D_L) = \frac{\exp[-(\tilde{\mathbf{v}}_L/\sigma(D_L))^2/2]}{2\pi[\sigma(D_L)]^2} \Lambda^{-5} D_{LS} \rho(D_L) \sqrt{\frac{D_L D_{LS}}{D_S}}. \quad (18)$$

The velocity dispersion is now given by

$$\sigma(D_L) = \frac{v_{\text{rot}}}{\sqrt{2}} \frac{D_S}{D_{LS}}, \quad (19)$$

with $v_{\text{rot}} = 220 \text{ km s}^{-1}$. Here, D_L and $D_S = 60 \text{ kpc}$ are the distances to the lens and the source, while $D_{LS} \equiv D_S - D_L$. The extra σ^{-2} factor in equation (18) is due to the fact that we cannot ignore the normalization of each Gaussian in this case. Note that in equation

(18), \tilde{v}_L is regarded as an implicit function of $\mathbf{\Lambda}$, which must be made explicit in order to quantitatively evaluate equation (17). Also note that there is an extra factor of D_{LS} on equation (18), since the probability should be weighted by v and not by \tilde{v} , as was done in the previous section.

The second consideration we must take into account for halo lensing is the effect of the motion of the Sun and the source on the projected velocity of the lens. In equation (18) we are assuming that the velocity distribution of the lenses is isotropic in the Galactic frame but we must also include the velocity offset induced by the motion of the Sun and the SMC with respect to the Galaxy. The three dimensional velocity of the Sun in UVW coordinates in the Galactic frame was measured by Hogg et al. (2005) to be

$$\mathbf{v}_\odot = (10.1, 224, 6.7) \text{ km s}^{-1}, \quad (20)$$

where U points from the Sun to the Galactic center, V points towards the Sun's Galactic rotation and W points towards the Galactic north pole. The velocity of the SMC is not well measured, but since it is most probably orbiting the LMC, it should have a very similar three dimensional velocity. Hence, we adopt the three dimensional velocity of the LMC for the SMC, which was measured by Kallivayalil et al. (2005) to be

$$\mathbf{v}_{\text{SMC}} = (-86, -268, 252) \text{ km s}^{-1}, \quad (21)$$

in the same coordinates system. Projected on celestial north and east coordinates, these velocities are

$$(\mathbf{v}_{\odot, N}, \mathbf{v}_{\odot, E}) = (119, -133) \quad (22)$$

$$(\mathbf{v}_{\text{SMC}, N}, \mathbf{v}_{\text{SMC}, E}) = (-296, 229). \quad (23)$$

The projected velocity of the lens relative to the observer-source line of sight is then

$$\tilde{\mathbf{v}} = \tilde{\mathbf{v}}_L - \tilde{\mathbf{v}}_0(D_L), \quad (24)$$

with

$$\tilde{\mathbf{v}}_0(D_L) \equiv \mathbf{v}_\odot + \frac{D_L}{D_{LS}} \mathbf{v}_{\text{SMC}}. \quad (25)$$

Solving equation (24) for \tilde{v}_L and substituting into equation (18), we find that for the positive u_0 solution, the ratios of the mean likelihood parameters of the SMC to the halo are 7 and 3 for the larger and smaller velocity dispersion respectively, while for the negative u_0 solution they are 3 and 2 respectively. This means that while SMC self lensing is somewhat favored, neither of the locations can be ruled out with good confidence.

In the left panel of Figure 4 we show the $\mathbf{\Lambda}$ probability distribution for halo lenses magnifying stars in the SMC, integrated over all D_L . There are two probability peaks with

similar Λ (or speed) but roughly opposite direction. This is due to the velocity offset, which flips sign as D_L increases. Also, for completeness of the statistical method proposed in this paper, we show in the right panel of Figure 4 the same probability distribution but for halo lenses causing microlensing events toward the LMC, in which an asymmetric probability peak can also be seen.

It should be noted that throughout this statistical test, we have assumed that there is equal prior probability that a microlensing event is caused either by self lensing or by halo lensing. There is no evidence for assuming something different, so the ratio of the mean likelihood parameters is actually the ratio of the probabilities of having this event caused by self lensing and by halo lensing.

6. EROS Fixed Blending

OGLE observations showed the presence of an optical companion to the source of MA-CHO 97-SMC-1 that was unresolved by EROS. Udalski et al. (1997b) estimated the light contribution of the companion to be 23%–28% of the total I band flux. This compares with 28 ± 12 % for the fits shown in Table 2, which tends to confirm that the OGLE-resolved source is the true microlensed source (although it remains possible in principle that there is a small component of blended light within this source). In this section we therefore assume that the blended flux in the EROS I_E band is exactly 24% and repeat the analysis of § 4. Such a strong constraint should remove the degeneracy between f_b and $\pi_{E,\perp}$, perhaps leading to a better determination of the lens location.

Refitting the model described in § 3 under this assumption, we obtain the χ^2 contours of the parallax parameters for both ($\pm u_0$) solutions shown on Figure 5. Both sets of contours are significantly less elongated in the $\pi_{E,\perp}$ direction when compared to their analogs in Figure 2, showing that the degeneracy is mostly broken, as expected.

A better constraint on the microlensing parallax allows for a better constraint on the projected velocity. Following the analysis detailed in § 5, we show the χ^2 contours for the components of vector Λ in Figure 6. These contours are also strongly compressed, so a better determination of the location of the lens might be possible.

Employing the statistical test detailed in § 5, we find that, for the positive u_0 solution, SMC self lensing is favored by factors of 27 and 33 for the larger and smaller SMC assumed velocity dispersions respectively. However, for the negative u_0 solution we find that the factors are 1 and 3, respectively. This result is very important, since it shows that even if we impose a strong constraint on the blended light, the location of the lens cannot be

determined with good confidence for this event.

7. Discussion

Variable stars are systematically eliminated from microlensing studies, but if one of them undergoes a microlensing event, its variability might actually be useful to constrain the event’s nature.

One such an event, MACHO 97-SMC-1, passed the variable-star cuts used by the MACHO and EROS collaborations. Using several data sets of this event taken by the MACHO, EROS and OGLE collaborations, we have shown that if the magnified source star is a regular variable, the parallax parameter in the direction perpendicular to the projected position of the Sun, $\pi_{E,\perp}$, can be constrained much better than if it were not a variable: the variability breaks the degeneracy between $\pi_{E,\perp}$ and the blended light. Figure 2 shows that, if we remove the variability from both the model and the data, the width of the π_E contours are almost doubled in the $\pi_{E,\perp}$ direction while they remain constant in the $\pi_{E,\parallel}$ direction.

We have proposed a statistical test to discriminate between the possible lens locations (halo or SMC) based on their velocity distributions and the χ^2 contours of $\mathbf{\Lambda}$, the inverse of the projected velocity. For MACHO 97-SMC-1, the test revealed that the lens is more likely to be located in the SMC itself rather than in the Galactic halo but that it is not possible to rule out the latter location. This test might be useful to discriminate quantitatively between possible lens locations of other microlensing events for which a parallax measurement can be performed.

We also showed that, even imposing a strong constraint on the flux, indicated by OGLE observations, the location of the lens still cannot be determined with good confidence.

We wish to thank Alejandro Clocchiatti for providing us with a spectrum of the MACHO 97-SMC-1 source star. Work by RJA and AG was supported by grant AST-0452758 from the NSF. Support for OGLE was provided by Polish MEiN grant 2P03D02124, NSF grant AST-0204908 and NASA grant NAG5-12212. DLW acknowledges research support from the Natural Sciences and Engineering Research Council of Canada (NSERC) in the form of a Discovery Grant.

This paper utilizes public domain data obtained by the MACHO Project, jointly funded by the US Department of Energy through Lawrence Livermore National Laboratory under contract W7405-ENG-48, the National Science Foundation through the Center for Particle Astrophysics of the University of California under cooperative agreement AST-8809616, and

the Mount Stromlo and Siding Springs Observatory by the Bilateral Science and Technology Program of the Australian Department of Industry, Technology and Regional Development.

A. MACHO 97-SMC-1 as an Ellipsoidal Variable

Udalski et al. (1997b) suggested that the source star is an ellipsoidal binary system, based on its nearly sinusoidal variations. In such systems, the binary separation is very small, and either one or both components are ellipsoidally distorted. Due to the interactions between them, their rotation and orbital periods are usually synchronized and the orbits are most likely circularized (see Beech 1985 and references therein). The star appears brighter at quadrature than at conjunction for two reasons. First, it has a larger surface area facing the observer. Second, the mean surface gravity of the exposed area is higher, implying that the surface is hotter and thus has a higher surface brightness. This leads to sinusoidal variations with a period equal to half of the orbital period.

Sahu & Sahu (1998) showed that, if MACHO 97-SMC-1 is a binary system, it is a single-lined spectroscopic one. As outlined by Morris (1985) and reviewed and updated by Morris & Naftilan (1993), it is possible to estimate the mass of the secondary star as well as its radius and other orbital parameters for a single-lined spectroscopic ellipsoidal binary using its light curve, the mass of the primary and its radial velocities (for double-lined spectroscopic binaries the mass of the primary can also be derived). The companion star should be dim enough to not be detected in the spectrum but massive enough to produce an ellipsoidal distortion on the primary.

To relate the amplitude of ellipsoidal variations to the binary parameters, we use equation (6) of Morris (1985),

$$\frac{qR_1^3 \sin^2 i}{A^3} = \frac{3.070 \Delta M_1 (3 - u_1)}{(\tau_1 + 1)(15 + u_1)}, \quad (\text{A1})$$

where q is the binary mass ratio (m_2/m_1), i is the orbital inclination, R_1 is the mean radius of the primary, A is the semi-major axis of the orbit, ΔM_1 is the mean peak-to-peak amplitude of the primary star alone, u_1 is the linear limb-darkening coefficient for the primary and τ_1 is its gravity darkening coefficient. These last two parameters (τ_1 and u_1) depend on the wavelength of the observation, λ . In our specific evaluation we will assume a V_E filter, but note that the results are essentially independent of this assumption. Equation (6) of Morris (1985) is accurate to first order and will suffice for this analysis. A more exact version of this equation is given by Morris & Naftilan (1993).

From its position on the color-magnitude diagram (Fig. 7) the source is a late B main

sequence star (see also Palanque-Delabrouille et al. 1998; Sahu & Sahu 1998) with an approximate mass of $5 M_{\odot}$. Using the empirical calibration of van Belle (1999) between the angular diameter and the $(V - K)$ color yields $R_1 \approx 5R_{\odot}$ if we assume that the value of $(V - K)$ is twice the value of $(V - I) = -0.05$ and that $D_{\text{SMC}} = 60$ kpc. Theoretical models predict a 15% smaller radius, but this will not be important for the results of this analysis. The orbital period P should be twice the variability period, so $P = 10.2$ days according to the variability period found in § 4.

According to the tables of Al-Naimiy (1978), for the V_E filter $u_1 \approx 0.35$, while τ_1 is given by equation (10) of Morris (1985)

$$\tau_1 = \beta \frac{1.43879 \times 10^8 / \lambda T_1}{1 - \exp(-1.43879 \times 10^8 / \lambda T_1)} \quad (\text{A2})$$

where T_1 is the effective temperature of the primary star (14000K in this case, Sahu & Sahu 1998), λ is in \AA and $\beta = 0.25$ for early type stars (von Zeipel’s Law, von Zeipel 1924), and yields $\tau_1 = 0.55$. Using Keplers Third Law to eliminate A in equation (A1) and solving for ΔM_1 , we find that

$$\Delta M_1 = 0.0094 \sin^2 i \left(\frac{R_1}{5R_{\odot}} \right)^3 \left(\frac{m_1}{5M_{\odot}} \right)^{-1} \left(\frac{P}{10.2 \text{days}} \right)^{-2} \frac{m_2}{m_1 + m_2} \quad (\text{A3})$$

From Table 2, $\Delta M_1 \approx [5/\ln(10)] \epsilon_{V_E} = 0.063$ mag for the “ V_E ” filter. If we adopt the most extreme mass parameters, $m_2 \gg m_1$ and $i = 90^\circ$, the right-hand side must increase by a factor of 7 from our estimate to reproduce the observed ΔM_1 .

This type of binary system should also present xallarap distortions on its microlensing events light curve. In order to test this, we fitted the data with a standard microlensing model with xallarap and variability but no parallax and found out that, to the $3\text{-}\sigma$ level, $\chi_E < 0.015$, where χ_E is the xallarap parameter,

$$\chi_E = \frac{a_1}{\hat{r}_E}. \quad (\text{A4})$$

That is, χ_E is the semi-major axis of the primary component, a_1 , in units of the Einstein ring radius projected in the plane of the source, \hat{r}_E . This small xallarap tends to reinforce the idea that MACHO 97-SMC-1 is not a binary system and is therefore not an ellipsoidal variable. However, the small xallarap might simply be caused by a very large Einstein ring projected on the source plane, which cannot currently be ruled out since the location of the lens cannot be determined with good confidence.

REFERENCES

- Afonso, C. et al. 1999, A&A, 344, L63
- Afonso, C. et al. 2003, A&A, 400, 951
- Alard, C., Mao, S., & Guibert, J. 1995, A&A, 300, L17
- Alcock C., et al. (MACHO collaboration) 1997, ApJ, 491, L11
- Alcock, C. et al. 2000, ApJ, 542, 281
- Al-Naimiy H. M. 1978, Ap&SS, 53, 181
- An, J.H. et al. 2002, ApJ, 572, 521
- An, J.H. et al. 2004, ApJ, 601, 845
- Beech, M. 1985, Ap&SS, 117, 69
- Boutreux, T. & Gould, A. 1996, ApJ, 462, 705
- Einstein, A. 1936, Science, 84, 506
- Ghosh, H. et al. 2004, ApJ, 615, 450
- Gould, A., Miralda-Escudé & Bahcall, J.N. 1994, ApJ, 423, L105
- Gould, A. & An, J.H. 2002, ApJ, 565, 1381
- Gould, A. 2004, ApJ, 606, 319
- Han, C. 1997, ApJ, 490, 51
- Hogg, D., Blanton, M., Roweis, S. & Johnston, K. 2005, ApJ, 629, 268
- Kallivayalil et al. 2005, ApJ, 638, 772
- Morris, S.L. 1985, ApJ, 295, 143
- Morris, S.L. & Naftilan, S.A. 1993, ApJ, 419, 344
- Paczyński, B. 1986, ApJ, 304, 1
- Palanque-Delabrouille, N., et al. 1998, A&A, 332, 1
- Park, B.-G. et al. 2004, ApJ, 609, 166

- Poindexter, S., Afonso, C., Bennett, D.P., Glicenstein, J.-F., Gould, A. Szymański, M., & Udalski, A. 2005, *ApJ*, 633, 914
- Refsdal, S. 1966, *MNRAS*, 134, 315
- Sahu, K. & Sahu, M.S. 1998, *ApJ*, 508, L147
- Smith, M. et al. 2003, *MNRAS*, 339, 925
- Tisserand, P. 2005, in *Semaine de l’Astrophysique Francaise*, ed. F. Casoli et al. (Les Ulis: EDP Sciences), 569.
- Udalski, A. 2003, *Acta Astron.*, 53, 291
- Udalski, A., Kubiak, M. & Szymański, M. 1997a, *Acta Astron.*, 47, 319
- Udalski et al. 1997b, *Acta Astron.*, 47, 431
- van Belle, G.T. 1999, *PASP*, 111, 1515
- von Zeipel, H. 1924, *MNRAS*, 84, 702
- Wyrzykowski, L., et al. 2006, *Acta Astron.*, 56, 145

Observatory	Filter	$u_0 > 0$	$u_0 < 0$	$u_0 > 0$ NoVar	$u_0 < 0$ NoVar
MACHO	V_M	306.6	306.5	305.6	305.9
	R_M	1057.7	1056.7	1052.0	1053.1
EROS	V_E	724.5	724.5	724.5	724.6
	I_E	841.0	841.9	843.8	844.1
MACHO CTIO	R	74.9	75.0	75.9	75.6
OGLE II	I	315.9	315.9	316.4	316.2
OGLE III	I	367.3	367.3	367.3	367.3
Total		3688.0	3687.8	3685.5	3686.9

Table 1: χ^2 for each filter (for each observatory) for the different models and solutions. NoVar indicates the case for which the best fitted variability of the star has been taken out from the data. Note that, because of round-off, in some cases the χ^2 of the filters/observatories do not add exactly to the total.

	$u_0 > 0$		$u_0 < 0$		$u_0 > 0$ NoVar		$u_0 < 0$ NoVar	
	Best Fit	Error	Best Fit	Error	Best Fit	Error	Best Fit	Error
t_0 (days)	1460.041	0.338	1459.936	0.385	1460.014	0.329	1459.910	0.428
u_0	0.419	0.048	−0.423	0.046	0.239	0.071	−0.344	0.077
t_E (days)	124.299	9.780	129.059	13.689	188.727	44.494	158.647	37.382
$\pi_{E,N}$	−0.017	0.011	−0.028	0.020	−0.057	0.015	−0.059	0.032
$\pi_{E,E}$	−0.002	0.003	−0.005	0.009	−0.004	0.003	−0.005	0.008
Ω (rad/days)	1.226	0.000	1.226	0.000				
$t_{0,\epsilon}$ (days)	2.539	0.025	2.540	0.025				
MACHO								
f_{s,V_M}	0.550	0.090	0.557	0.088	0.259	0.096	0.417	0.128
f_{b,V_M}	0.253	0.090	0.246	0.088	0.543	0.096	0.385	0.127
ϵ_{V_M}	0.029	0.004	0.028	0.004				
f_{s,R_M}	0.861	0.141	0.871	0.138	0.405	0.151	0.653	0.200
f_{b,R_M}	0.360	0.141	0.350	0.137	0.815	0.150	0.568	0.200
ϵ_{R_M}	0.023	0.003	0.023	0.003				
EROS								
f_{s,V_E}	0.532	0.087	0.539	0.085	0.251	0.093	0.403	0.124
f_{b,V_E}	0.236	0.087	0.230	0.085	0.518	0.093	0.365	0.124
ϵ_{V_E}	0.029	0.005	0.029	0.005				
f_{s,I_E}	1.226	0.201	1.241	0.196	0.577	0.215	0.929	0.285
f_{b,I_E}	0.487	0.201	0.473	0.196	1.136	0.215	0.784	0.285
ϵ_{I_E}	0.024	0.004	0.024	0.004				
MACHO CTIO								
$f_{s,R}$	24.133	4.126	24.426	3.950	11.384	4.134	18.351	5.581
$f_{b,R}$	7.277	4.155	6.965	3.967	20.026	4.101	13.032	5.574
ϵ_R	0.030	0.005	0.029	0.005				
OGLE II								
$f_{s,I}$	0.734	0.128	0.737	0.127	0.347	0.134	0.551	0.174
$f_{b,I}$	0.204	0.129	0.201	0.127	0.590	0.133	0.386	0.174
ϵ_I	0.031	0.006	0.031	0.006				
OGLE III								
$f_{s,I}$	0.684	0.001	0.684	0.001	0.684	0.001	0.684	0.001
$f_{b,I}$	0.254		0.254		0.254		0.254	
ϵ_I	0.033	0.003	0.033	0.003				

Table 2: Best fit parameters with their respective errors for the different models and solutions. NoVar indicates the case for which the best fitted variability of the star has been taken out from the data. $t_{0\epsilon}$ is defined as ϕ/Ω , where ϕ is the phase defined in equation (10). The time of the maximum, t_0 , is measured in $JD - 2449000$, while the fluxes are measured in arbitrary units. The seemingly excessive number of decimal places included for each parameter are potentially important to reproduce these results, because the correlations among some parameters are high.

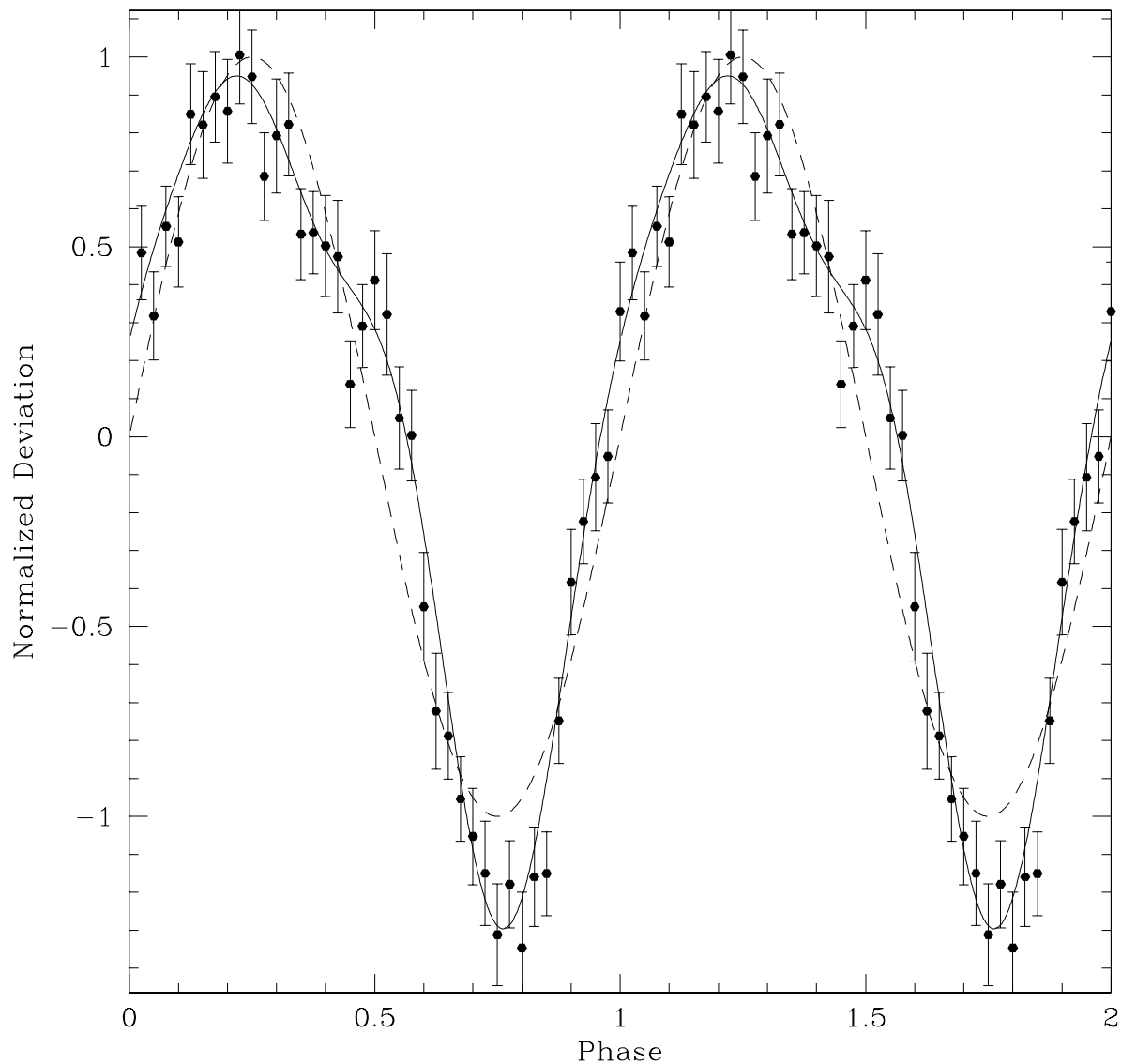


Fig. 1.— Variability light curve of MACHO 97-SMC-1, derived from the residuals of the fit of equation (10) with $G(x) = \sin(x)$. The solid curve shows the variability model used in this analysis, which correspond to a fourth-order Fourier expansion fit of the residuals, while the dashed line shows a sine function, the model used by Palanque-Delabrouille et al. (1998).

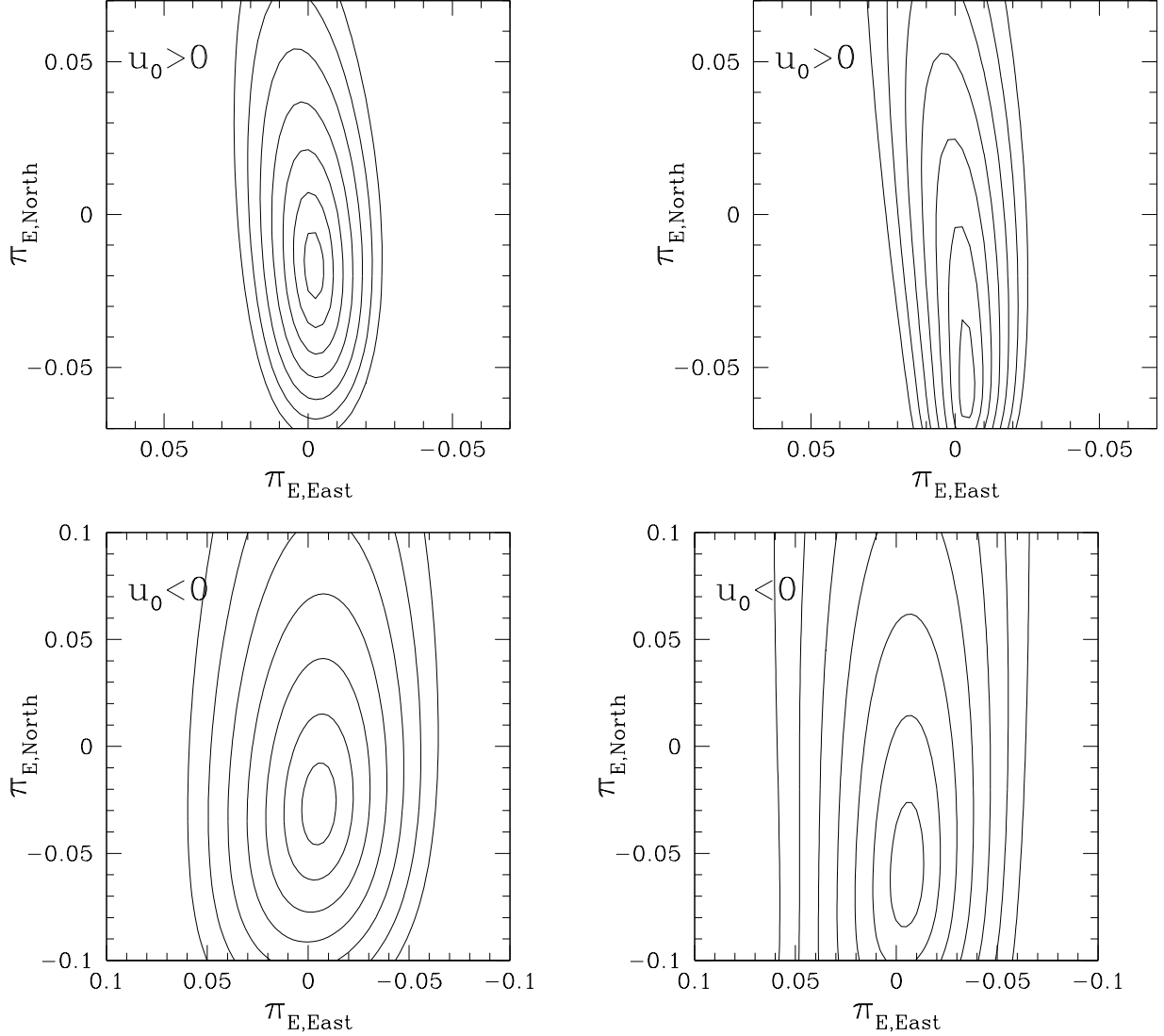


Fig. 2.— $\Delta\chi^2$ contours (1,4,9,16,25,36,49) of the parallax parameters for positive (top) and negative (bottom) u_0 . The plots on the left show these contours for the model described in § 3, a standard microlensing model with parallax and taking into account the variability of the source, while the ones on the right shows the parallax χ^2 contours for the same model but with the variability removed from both the data and the model. The contours on the right are strongly stretched in the direction of $\pi_{E,\perp}$ (which coincides almost exactly with $\pi_{E,N}$) compared to the ones on the left, showing that the variability of the source breaks the degeneracy between $\pi_{E,\perp}$ and $f_{b,k}$, allowing to constrain much better the parallax.

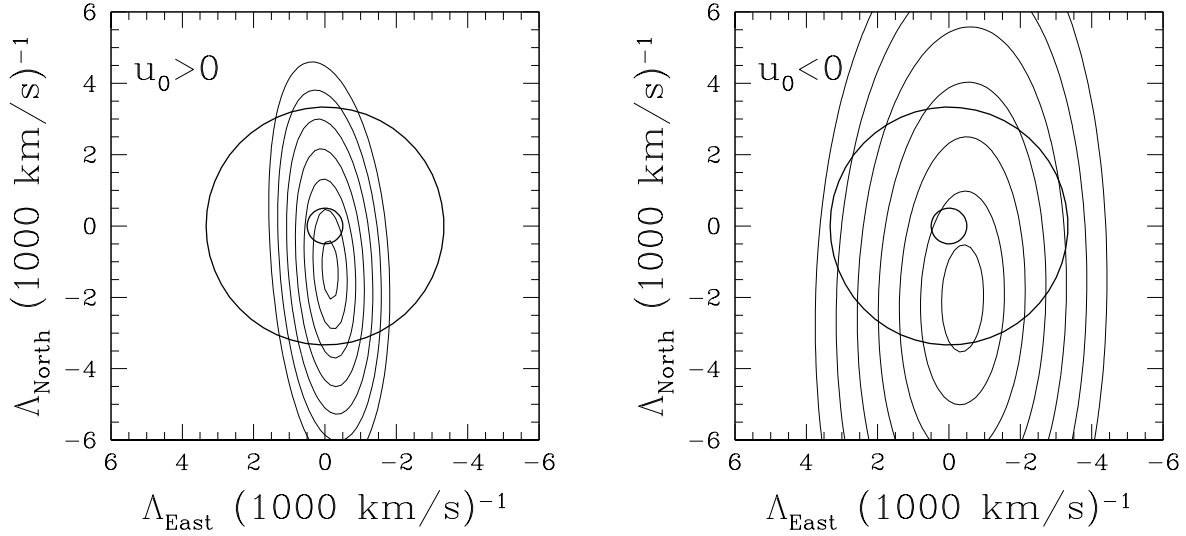


Fig. 3.— $\Delta\chi^2$ contour (1,4,9,16,25,36,49) plots for Λ , the inverse of the projected velocity (in km s^{-1}), for both $\pm u_0$ solutions. The small circle in the middle shows a projected velocity (in the frame of the Sun) of 2000 km s^{-1} while the other circle shows 300 km s^{-1} , typical projected velocities for SMC and halo lenses, respectively.

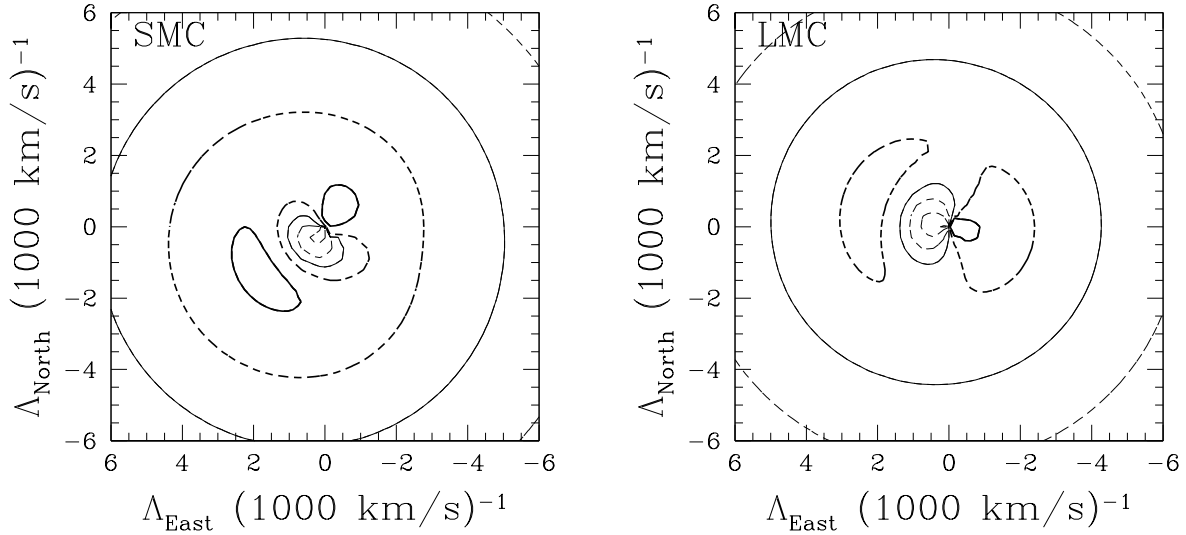


Fig. 4.— Inverse projected velocity Λ probability distribution of halo lenses causing microlensing events toward the SMC (left) and the LMC (right). The velocity offset discussed in § 5.2 makes the distributions highly asymmetric, contrary to the case for SMC self lensing. The contour levels are offset from one another by a factor of 5, with order, highest to lowest, bold solid, bold dashed, thin solid and thin dashed (of which there are several).

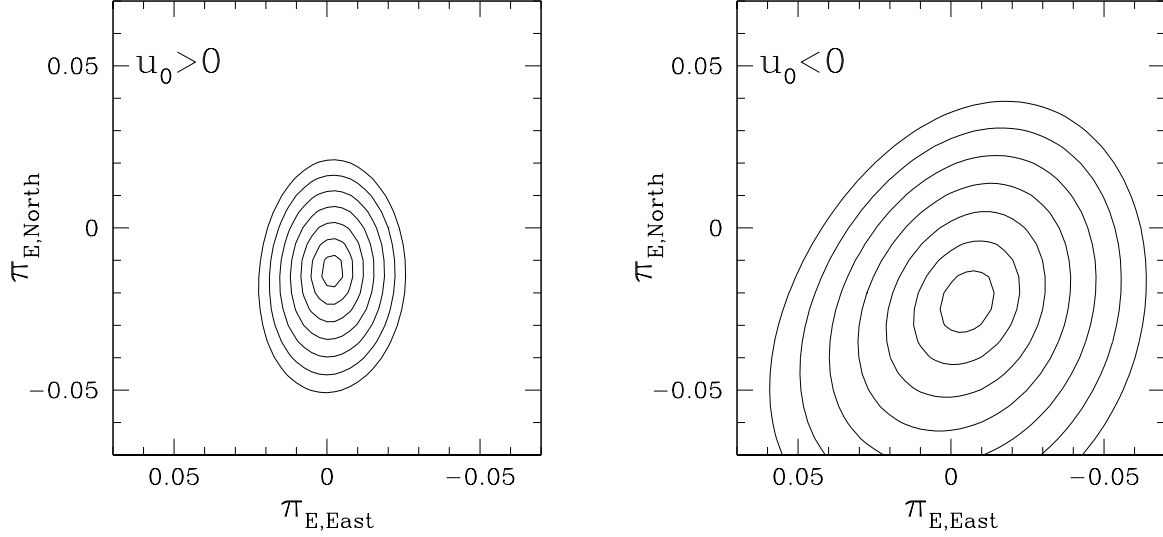


Fig. 5.— $\Delta\chi^2$ contours (1,4,9,16,25,36,49) for the parallax parameters assuming that 24% of the light detected in the EROS I_E band is due to blending. Compared to the left contours in Figure 2, they are strongly compressed in the $\pi_{E,\perp}$ direction, showing that by this assumption the degeneracy between f_b and $\pi_{E,\perp}$ is almost completely eliminated.

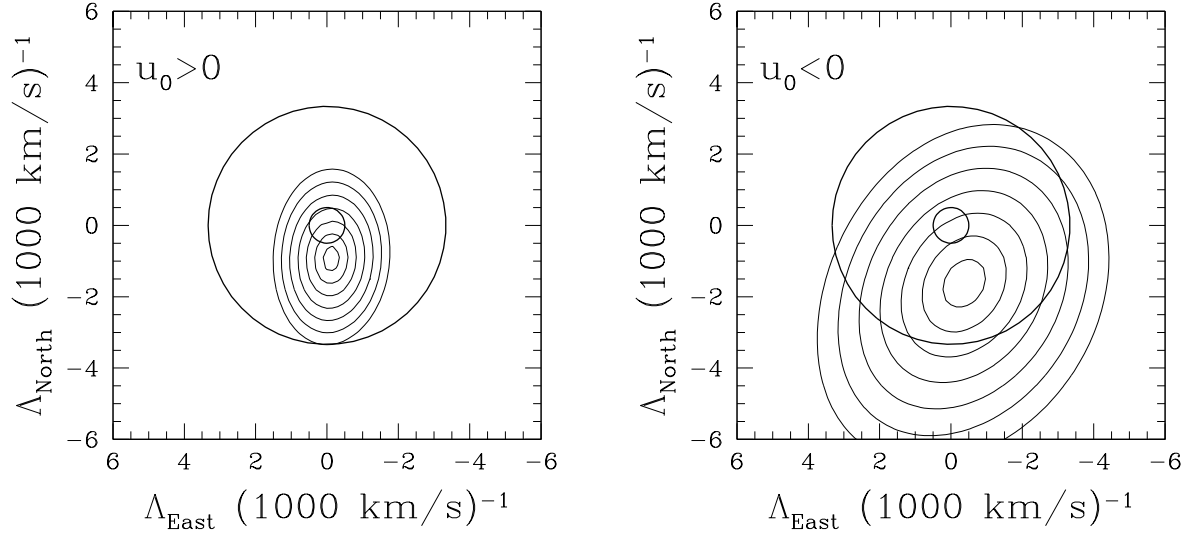


Fig. 6.— $\Delta\chi^2$ contours (1,4,9,16,25,36,49) for Λ assuming that 24% of the light in the EROS I_E band is due to a blend. As discussed in § 6, even though the contours are now nearly circular, the location of the lens cannot be determined with good confidence.

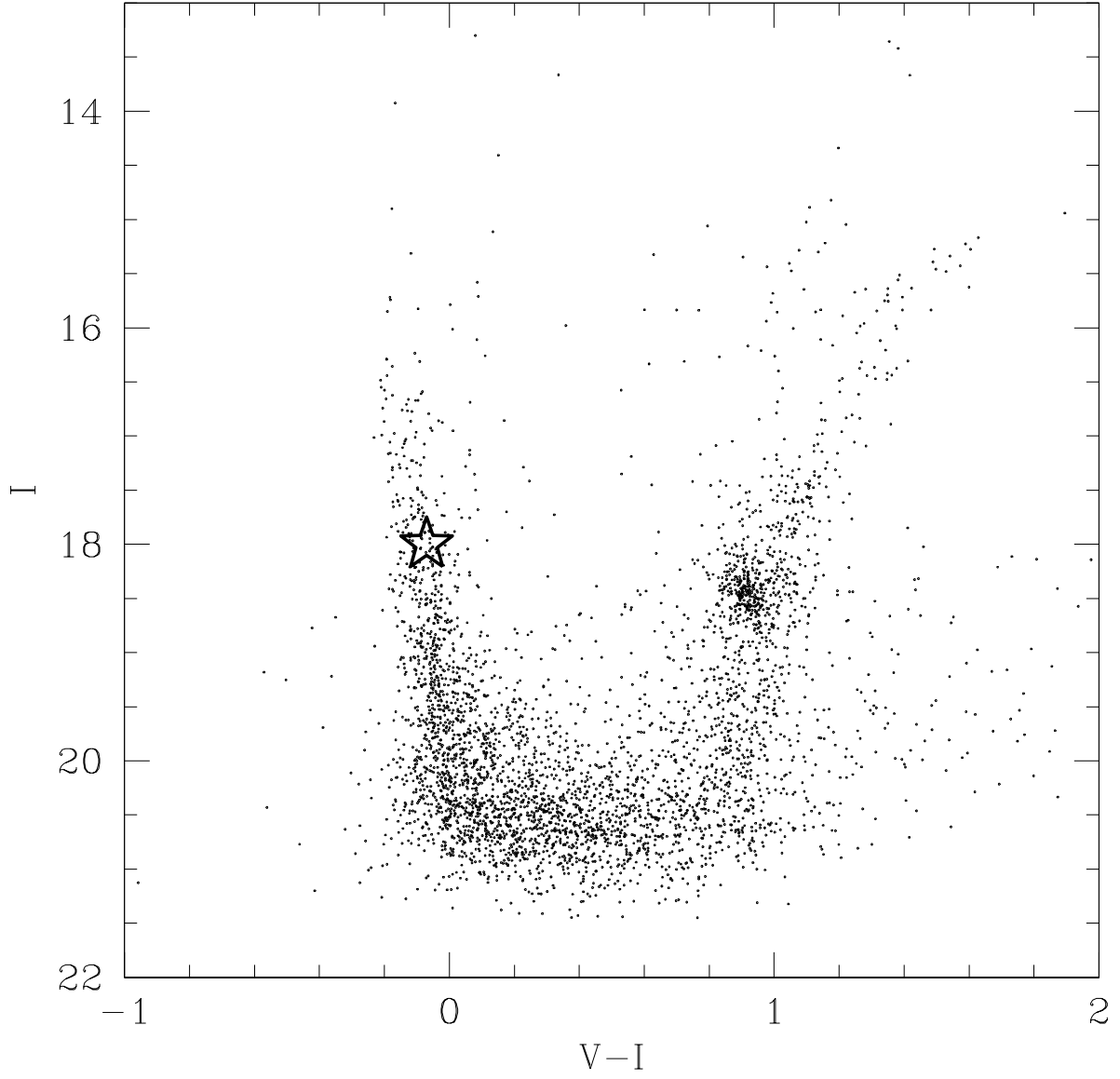


Fig. 7.— Color Magnitude Diagram of the OGLE-II SMC field centered on MACHO 97-SMC-1. The star marks the position of the source of the MACHO 97-SMC-1 event. This indicates that it is a late B main sequence star, compatible with the spectroscopic determination of Sahu & Sahu (1998).